Cancer Letters 453 (2019) 95–106

Contents lists available at ScienceDirect

Cancer Letters

journal homepage: www.elsevier.com/locate/canlet

Original Articles

Metastasis of pancreatic cancer: An uninflamed liver micromilieu controls cell growth and cancer stem cell properties by oxidative phosphorylation in pancreatic ductal epithelial cells

Alexander Fabian[a], Simon Stegner[a], Lauritz Miarka[a], Johannes Zimmermann[b], Lennart Lenk[c], Sascha Rahn[a], Jann Buttlar[a], Fabrice Viol[d], Hendrike Knaack[a], Daniela Esser[b], Sascha Schäuble[e], Peter Großmann[e], Georgios Marinos[b], Robert Häsler[f], Wolfgang Mikulits[g], Dieter Saur[h], Christoph Kaleta[b], Heiner Schäfer[a], Susanne Sebens[a,*]

[a] Group Inflammatory Carcinogenesis, Institute for Experimental Cancer Research, Christian-Albrechts-University Kiel and University Hospital Schleswig-Holstein (UKSH) Campus Kiel, Arnold-Heller-Str. 3, Building 17, 24105, Kiel, Germany
[b] Group Medical Systems Biology, Institute for Experimental Medicine, Michaelisstr. 5, Building 17, 24105, Kiel, Germany
[c] Department of Pediatrics, Christian-Albrechts-University Kiel and University Medical Center Schleswig-Holstein, Schwanenweg 20, 24105, Kiel, Germany
[d] Department of Medicine I, University Medical Center Hamburg-Eppendorf, Hamburg, Germany
[e] Leibniz Institute for Natural Product Research and Infection Biology, Hans Knöll Institute (HKI), Beutenbergstraße 11A, 07745, Jena, Germany
[f] Group Molecular Cell Biology, Institute of Clinical Molecular Biology, Christian-Albrechts-University Kiel, Rosalind-Franklin-Straße 12, 24105, Kiel, Germany
[g] Department of Medicine I, Division: Institute of Cancer Research, Comprehensive Cancer Center, Medical University of Vienna, Vienna, Austria
[h] II. Medizinische Klinik und Poliklinik, Klinikum Rechts der Isar, Technical University Munich, Munich, Germany

ARTICLE INFO

Keywords:
Pancreatic cancer
Metastases
Cancer stemness
Metabolism
Liver microenvironment

ABSTRACT

Pancreatic ductal adenocarcinoma (PDAC) is commonly diagnosed when liver metastases already emerged. We recently demonstrated that hepatic stromal cells determine the dormancy status along with cancer stem cell (CSC) properties of pancreatic ductal epithelial cells (PDECs) during metastasis. This study investigated the influence of the hepatic microenvironment – and its inflammatory status - on metabolic alterations and how these impact cell growth and CSC-characteristics of PDECs. Coculture with hepatic stellate cells (HSCs), simulating a physiological liver stroma, but not with hepatic myofibroblasts (HMFs) representing liver inflammation promoted expression of Succinate Dehydrogenase subunit B (SDHB) and an oxidative metabolism along with a quiescent phenotype in PDECs. SiRNA-mediated SDHB knockdown increased cell growth and CSC-properties. Moreover, liver micrometastases of tumor bearing KPC mice strongly expressed SDHB while expression of the CSC-marker Nestin was exclusively found in macrometastases. Consistently, RNA-sequencing and *in silico* modeling revealed significantly altered metabolic fluxes and enhanced SDH activity predominantly in pre-malignant PDECs in the presence of HSC compared to HMF. Overall, these data emphasize that the hepatic microenvironment determines the metabolism of disseminated PDECs thereby controlling cell growth and CSC-properties during liver metastasis.

Abbreviations: BSA, bovine serum albumin; CFA, colony formation assay; CSCs, cancer stem cells; CK19, cytokeratin 19; ECAR, extracellular acidification rate; FCCP, carbonyl cyanide-4-(trifluoromethoxy)phenylhydrazone; FITC, fluorescein isothiocyanate; GAPDH, glyceraldehyde 3-phosphate dehydrogenase; G6PD, glucose-6-phosphate dehydrogenase; HMF, M-HT = hepatic myofibroblast cell line; HMFs, hepatic myofibroblasts; HRP, horseradish peroxidase; HSC, M1-4HSC = hepatic stellate cell line; HSCs, hepatic stellate cells; HSP90, heat shock protein 90; LDH, lactate dehydrogenase; LDHA/B, lactate dehydrogenase subunit A/B; MCT4, monocarboxylate transporter 4; OCR, oxygen consumption rate; OXPHOS, oxidative phosphorylation; PanIN, pancreatic intraepithelial neoplasia; PBS, phosphate buffered saline; PDAC, pancreatic ductal adenocarcinoma; PDECs, pancreatic ductal epithelial cells; PGD, phosphogluconate dehydrogenase; PPP, pentose phosphate pathway; SABG, senescence associated β-galactosidase; SDH, succinate dehydrogenase; SDHB, succinate dehydrogenase subunit B; TALDO, transaldolase; TBST, tris-buffered saline with tween 20; TCA, tricarboxylic acid; TGFβ, transforming growth factor β; TKT, transketolase; VEGF, vascular endothelial growth factor

* Corresponding author. Group Inflammatory Carcinogenesis, Institute for Experimental Cancer, Christian-Albrechts-University Kiel and UKSH Campus Kiel, Arnold-Heller-Str. 3, Haus 17, 24105, Kiel, Germany.
E-mail address: susanne.sebens@email.uni-kiel.de (S. Sebens).

https://doi.org/10.1016/j.canlet.2019.03.039
Received 25 October 2018; Received in revised form 8 March 2019; Accepted 21 March 2019

1. Introduction

Pancreatic ductal adenocarcinoma (PDAC) is currently ranked the fourth common cause of cancer related deaths in Europe [1]. It is characterized by the absence of specific symptoms and a high metastatic potential. Thus, PDAC is commonly diagnosed at advanced stages with liver metastases allowing only for palliative treatment. Moreover, many patients who successfully underwent surgical resection of the tumor develop metastases within one year [2]. The liver is the main target organ of PDAC metastases, already commencing at stages of Pancreatic Intraepithelial Neoplasia (PanIN) but without immediate outgrowth. Metastatic outgrowth apparently requires further (epi-)genetic alterations or changes in the local microenvironment [3]. Inflammatory factors released by primary pancreatic lesions seem to modulate the liver microenvironment leading to formation of the pre-metastatic niche [4–6]. This niche formation involves the activation and transdifferentiation of hepatic stellate cells (HSCs) into hepatic myofibroblasts (HMFs) [5,7]. Our group recently demonstrated that the hepatic microenvironment essentially determines growth behavior of disseminated pancreatic ductal epithelial cells (PDECs) [8]. Thus, PDECs became dormant in the presence of HSCs while this quiescent phenotype of PDECs was reversed and their proliferative activity was significantly restored in the presence of HMFs through a Vascular Endothelial Growth Factor (VEGF) dependent mechanism [8].

Due to the unique ability of self-renewal and differentiation, cancer stem cells (CSCs) are regarded as prerequisite for the initiation of primary tumors and metastases [9,10]. CSCs have also been described in PDAC [11] with different markers used for their identification and isolation such as Esa/CD44/CD24, CD133, Sox2, Nanog or Nestin [12–15]. Particularly Nestin has been described to play a pivotal role in PDAC progression because knockdown of Nestin significantly impaired PDAC cell invasion [15] and metastases formation in a murine PDAC model [16,17]. We have shown that PDAC cells with high CSC-potential are characterized by high Nestin expression [18].

Metabolic reprogramming is regarded as a hallmark of cancer essentially driving tumor development [19,20]. Otto Warburg first identified that tumor cells exhibit an altered glucose metabolism by shifting from oxidative phosphorylation (OXPHOS) to glycolysis with lactate production (aerobic glycolysis) [21]. Interconnected with this Warburg effect, tumor cells may activate further pathways to metabolize glucose and generate building blocks for enhanced DNA synthesis and redox homeostasis, e.g. the pentose phosphate pathway (PPP) with Glucose-6-phosphate dehydrogenase (G6PD) as the rate limiting enzyme [22,23]. Accordingly, elevated G6PD expression was detected in different tumors being associated with high risk of metastasis and poor prognosis [22,24,25]. Importantly, the metabolic status of tumor cells within a tumor is highly dynamic and depends on microenvironmental conditions (e.g. stromal composition, oxygen level) implying different metabolic phenotypes within tumor and stroma cell populations [26–32]. Succinate dehydrogenase (SDH) is an important mitochondrial enzyme involved in the tricarboxylic acid (TCA) cycle as well as the electron transport chain. The SDH subunit B (SDHB) being one of the four subunits of SDH is regarded as tumor suppressor because its mutational inactivation or its decreased expression is observed in several tumor entities [33,34]. Thus, adaptation of the metabolism in response to environmental conditions provides an essential mechanism for tumor cells to survive in a hostile (secondary) microenvironment. As for normal stem cells, a high metabolic flexibility is also mandatory for CSCs in order to allow the divergent cell fates including quiescence, proliferation and differentiation/reversal into non-CSCs [35]. However, our knowledge on how metabolic alterations impact cell growth and CSC-properties of PDECs is still limited, particularly in the metastatic context. Hence, this study elucidated the influence of the hepatic microenvironment –and its inflammatory status-on metabolic alterations and how these impact cell growth and CSC-characteristics of PDECs.

2. Material and methods

2.1. PDAC KPC model

All animal studies were executed in compliance with European guidelines for the care and use of laboratory animals and were approved by local authorities (Az. 55.2-1-54-2532-31-11). For HE- and immunofluorescence stainings of murine PDAC liver metastases, liver tissues of KPC mice (Pdx1-Cre; LSL-KrasG12D; LSL-Trp53R172H/+) were used.

2.2. HE- and immunofluorescence staining of liver sections

Staining procedures were performed as previously described [36]. Primary antibodies (Supplementary Table 1) were diluted in 1% BSA/PBS and incubated overnight at 4 °C. For staining of Nestin, an additional blocking step with Dako Biotin Blocking System (Dako, Hamburg, Germany) was performed according to manufacturer's instructions. Background intensity was reduced by application of Image-iT FX Signal Enhancer (Thermo Fisher Scientific, Darmstadt, Germany) according to the manufacturer's instructions. Then, slides were incubated for 1 h at room temperature with respective secondary antibodies (Supplementary Table 1) diluted in 1% BSA/PBS and Hoechst for detection of nuclei. Biotin-labeled antibodies were detected with FITC-conjugated streptavidin (Vector Laboratories via Biozol, Eching, Germany). Stainings were visualized on a BZ-9000 fluorescence microscope (Keyence; Neu-Isenburg, Germany) using the BIOREVO software (Keyence) and the LIONHEART FX Live Cell Imager (Biotek Instruments GmbH, Bad Friedrichshall, Germany) using the GEN5 software (Biotek). Picture analysis was performed as previously described [36].

2.3. Cell lines and cell culture

The human PDEC lines H6c7-pBp (benign, non-tumorigenic) and H6c7-kras (premalignant with limited tumorigenicity, both kindly provided by M.S. Tsao, Ontario Cancer Institute, Toronto, Canada [37]) were cultured as described [8,18]. The human PDAC cell line Panc1 was obtained from ATCC (LGC Standards, Wesel, Germany) and cultured as described [8,18]. The genotype of the cell lines was recently confirmed by Short Tandem Repeat Analysis. The murine hepatic stellate cell line M1-4HSC, representing a physiologic liver microenvironment and termed HSC, was cultured as previously described [8,38]. M-HT cells, being termed HMF, result from long-term exposition of M1-4HSC to 1 ng/ml TGFβ1 (BioLegend, Fell, Germany) and were cultured as described [8,38]. The latter cells were used to model an inflamed hepatic microenvironment.

2.4. Indirect coculture of hepatic stromal cells and PDECs

Using a transwell coculture system, indirect coculture of PDECs and HSC or HMF, respectively, was conducted for 6 days as described previously [8]. In this former study, coculture experiments with human PDECs and human hepatic stromal cells were performed, too, revealing similar findings and underscoring the validity of the coculture model [8].

2.5. SiRNA-mediated SDHB knockdown

One $x10^4$ PDECs/well were seeded in a 6-well plate and incubated at 37 °C, 5% CO_2 and 86% humidity for 24 h. Then, 12 µl HiPerFect (Qiagen, Venlo, NL) and 1 µl of either SDHB siRNA (sc-44088 containing three SDHB-specific 19–25 nucleotide siRNAs) or control siRNA-A (sc-37007, both from Santa Cruz Biotechnology, Heidelberg, Germany) were mixed and PDECs transfected following the manufacturer's protocol. After 8–12 h, medium was exchanged and coculture started for 6 days.

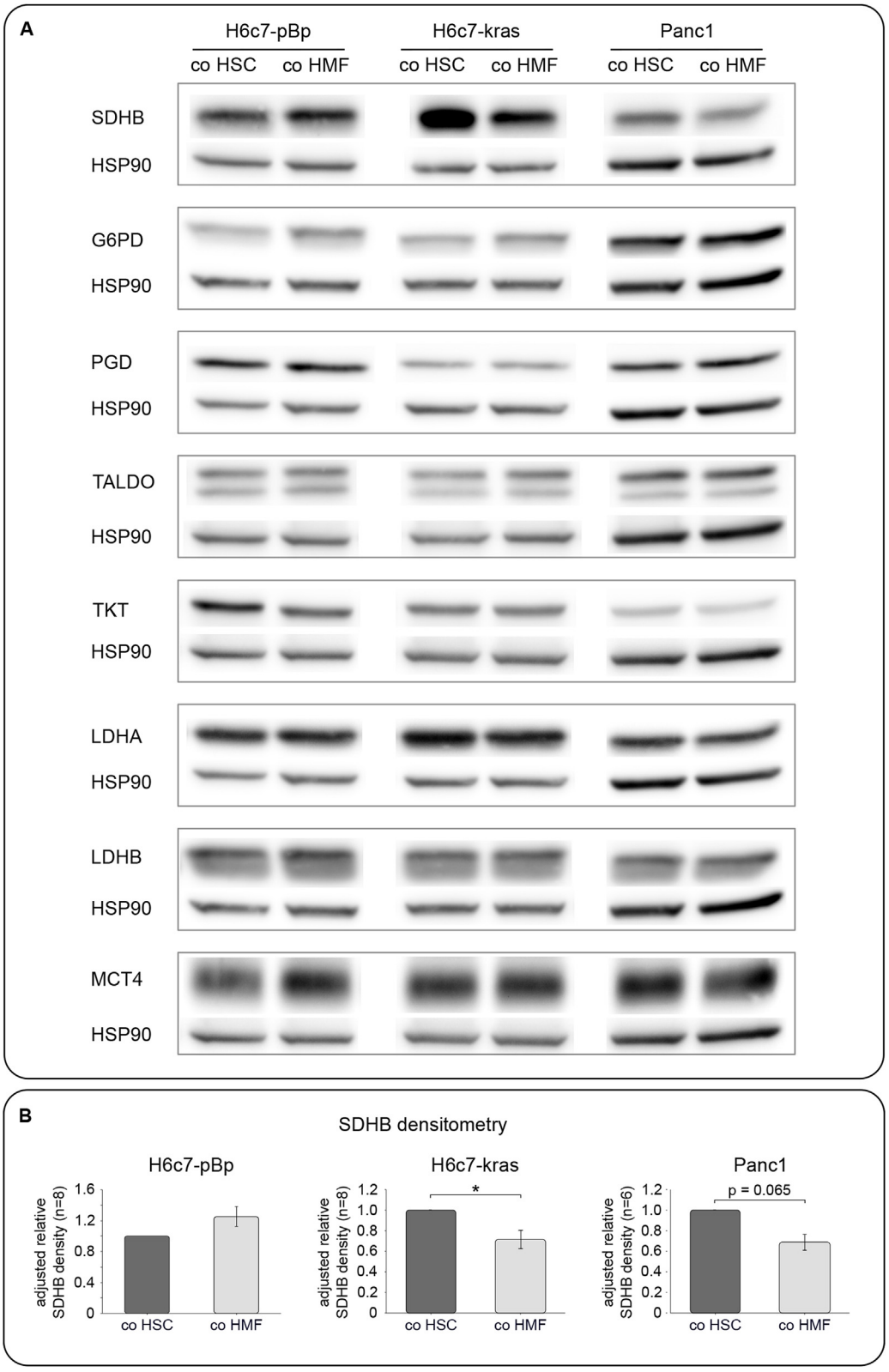

Fig. 1. Screening of metabolic enzymes reveals higher SDHB-expression in PDECs after HSC− compared to HMF-coculture. H6c7-pBp, H6c7-kras or Panc1 cells were indirectly cocultured (co) with HSC or HMF for 6 days and analyzed for expression of the indicated proteins by western blotting. HSP90 was used as loading control. **(A)** Representative western blots of 4–8 independent experiments are shown. **(B)** Densitometry of SDHB blots was performed using ImageJ. Relative densities of bands of SDHB expression were adjusted to the respective loading control and compared between HSC− or HMF-cocultured H6c7-kras or Panc1 cells, respectively. Results were normalized to HSC-coculture set as 1. Bars show mean ± SEM of 8 independent experiments in H6c7-pBp and H6c7-kras and 6 independent experiments in Panc1 cells. * = $p < 0.05$.

2.6. Determination of vital cell number

After detachment, cells were stained with trypan blue (Sigma-Aldrich, Munich, Germany) and counted using a Neubauer counting chamber. For quantification of vital cells, blue stained cells were excluded from counting.

2.7. Determination of senescence associated β-Galactosidase (SABG) activity

To determine the number of quiescent/senescent PDECs, the Senescence β-Galactosidase Staining Kit (Cell Signaling via New England Biolabs, Frankfurt/a.M., Germany) was utilized according to manufacturer's instructions.

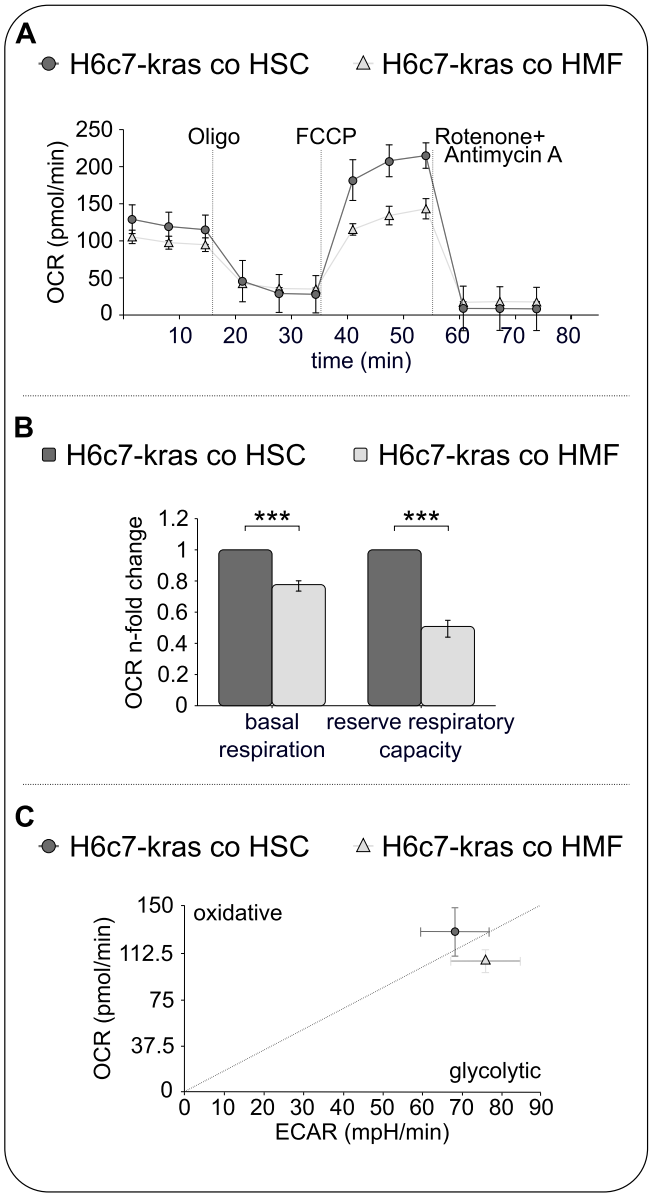

Fig. 2. PDECs display an increased oxidative metabolism in the presence of HSC compared to HMF. H6c7-kras cells were indirectly cocultured (co) with HSC or HMF for six days and then analyzed for real time oxygen consumption rate (OCR) and extracellular acidification rate (ECAR) using the XF Cell Mito Stress Test Kit on a Seahorse XFp Analyzer. **(A)** OCR during a course of 75 min modified by application of either Oligomycin, FCCP or Rotenone/Antimycin A. One representative out of three independent experiments is shown. **(B)** OCR of H6c7-kras cells cocultured with HSC was set as 1 and compared to HMF-coculture in terms of calculated basal respiration and reserve respiratory capacity. Bars show mean ± SEM of three independent experiments. *** = $p < 0.001$. **(C)** Metabolic phenotypes of differentially cocultured H6c7-kras cells characterized by intensity ratio of OCR and ECAR. One representative of three independent experiments is shown.

2.8. Immunofluorescence stainings of cultured PDECs

After removal of the medium, siRNA transfected and cocultured PDECs were washed in PBS and fixed with 4.5% paraformaldehyde for 15 min. Afterwards, cells were washed in PBS and permeabilized with ice-cold methanol + 0.3% H_2O_2 for 10 min at −20 °C. After washing in PBS, cells were blocked in 4% BSA in PBS/0.3% Triton X-100 (PBS/T) for 1 h at room temperature. Primary antibodies (Supplementary Table 1) were diluted in 1% BSA in PBS/T and incubated at 4 °C overnight. Then, cells were washed with PBS/T and incubated for 1 h at room temperature with the respective secondary antibodies (Supplementary Table 1) diluted in 1% BSA in PBS/T and Hoechst for detection of nuclei. After washing in PBS, coverslips containing stained cells were fixed on slides and covered with FluorSave reagent (Merck Millipore, Darmstadt, Germany). Stainings were visualized using a BZ-9000 fluorescence microscope (Keyence) and the BIOREVO software (Keyence).

2.9. Western blotting

Preparation of whole cell lysates, electrophoresis and western blotting were conducted as described [39,40]. Primary antibodies (Supplementary Table 2) were incubated overnight at 4 °C and detected by the respective HRP-linked secondary antibodies at room temperature for 1 h. After washing in TBST, blots were developed with SuperSignal West Dura Extended Duration Substrate (Perbio Sciences, Bonn, Germany).

2.10. Colony formation assay (CFA)

CFAs of cocultured PDECs were conducted as described previously [18]. Colonies consisting of more than 50 cells were considered as colony and counted. Additionally, the morphology of each colony was assessed as para-, mero- or holoclone representing increasing self-renewal capacity in this order [41,42].

2.11. Seahorse analysis

Oxygen consumption rate (OCR) and extracellular acidification rate (ECAR) of PDECs were measured using the XF Cell Mito Stress Test Kit on a Seahorse XFp Analyzer (both from Agilent, Santa Clara, USA). Cartridges were hydrated with 200 µl XF Calibrant and XFp Miniplates were coated using 50 µl poly-D-lysine (Sigma-Aldrich, St. Louis, USA) overnight. The following day, 3.5×10^4 of previously cocultured cells were seeded and spun in XFp Miniplates using XF Base Medium (supplemented with 10 mM D-glucose, 1 mM L-glutamine and 1 mM sodium pyruvate) and incubated in a non-CO_2 incubator at 37 °C for 1 h. The measurement was started and 1 µM Oligomycin (Oligo), 0.5 µM carbonyl cyanide-4-(trifluoromethoxy)phenylhydrazone (FCCP) and 0.5 µM Rotenone/Antimycin A were sequentially injected at indicated time points. Data were calculated by the XFp Analyzer software and normalized to baseline OCR.

2.12. RNA isolation and RT-PCR

Total RNA was isolated with the total RNA kit peqGOLD (Thermo Fisher Scientific) and subjected to reversed transcription making use of the RevertAid First Strand cDNA synthesis kit provided by Fermentas according to the manufacturer's instructions (Thermo Fisher Scientific). Primer sequences are displayed in Supplementary Table 3. PCR analyses were performed in duplicates with a LightCycler 480 (Roche, Mannheim, Germany) for a maximum of 50 cycles ending with a melting curve analysis as quality control. For relative quantification of mRNA levels C_T-values of genes of interest were normalized to the respective C_T-value of the housekeeping gene GAPDH.

2.13. RNA isolation and RNA-sequencing

Sequencing libraries were created with the TruSeq Stranded Total RNA Library Prep Kit from Illumina (San Diego, USA). Sequencing was performed with the Illumina TruSeq SBS Kit (51 cycles) on the Illumina HiSeq4000.

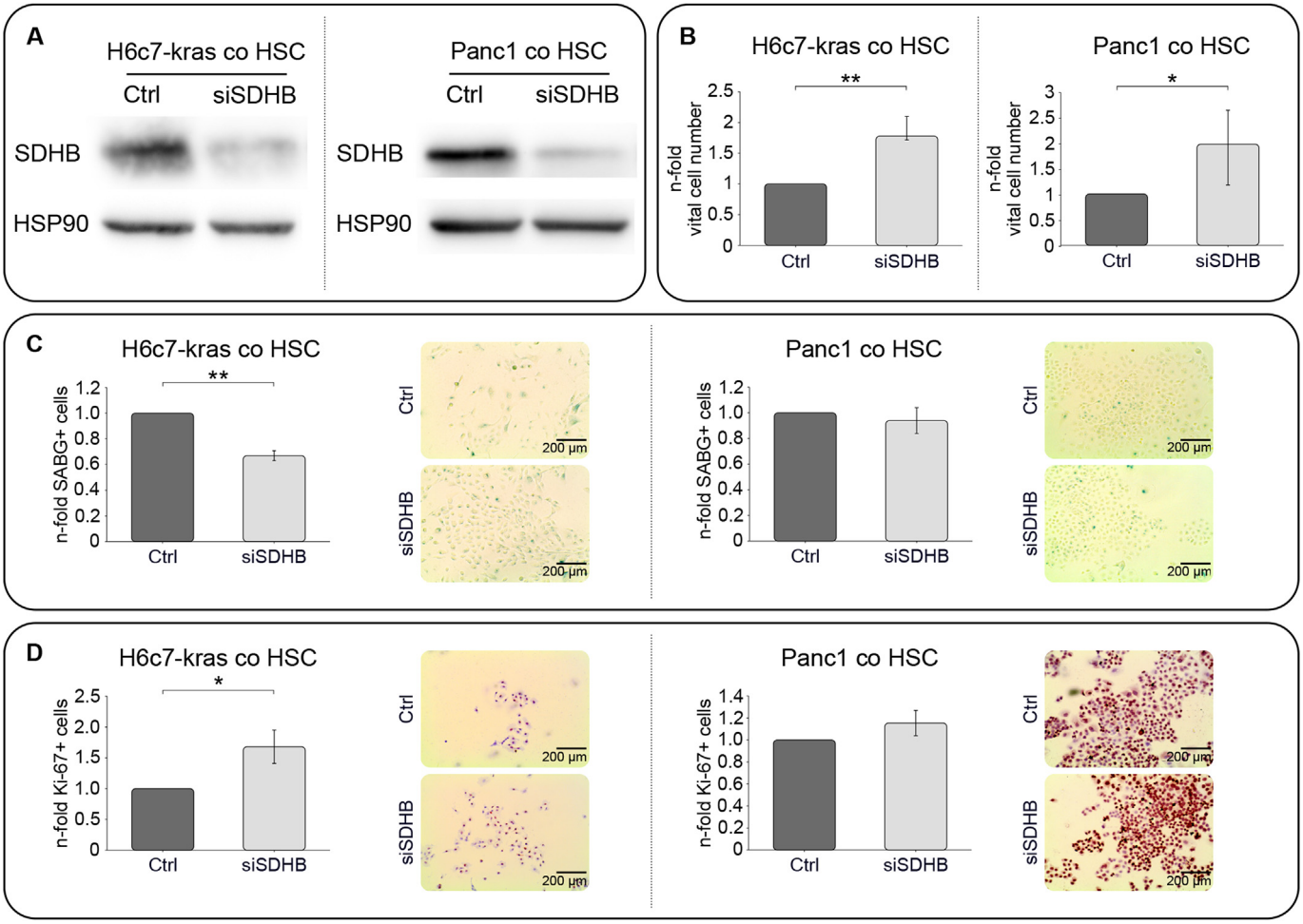

Fig. 3. SDHB determines cell growth behavior of PDECs. H6c7-kras or Panc1 cells were transfected with control siRNA (Ctrl) or SDHB siRNA (siSDHB) respectively. After one day, indirect coculture (co) with HSC was started and PDECs were analyzed after six days. **(A)** Expression levels of SDHB were determined by western blotting. HSP90 was used as loading control. Representative western blots of 5–6 independent experiments are shown. **(B)** Vital cell count of siSDHB transfected PDECs was normalized to control transfected cells. Bars display median ± quartiles ($Q_{0.75}$ as upper, $Q_{0.25}$ as lower deviation) of 4 independent experiments. **(C,D)** Percentage of SABG + and Ki67 + PDECs were normalized to respective control transfected cells. Bars represent mean ± SEM of three independent experiments. Representative images of SABG and Ki67 stainings are shown.
* = $p < 0.05$, ** = $p < 0.01$.

2.14. Generation of coculture condition-specific metabolic models

A generic genome-scale metabolic model of humans [43] served as a template for a data-driven model derivation. Gene expression data from PDECs after coculture with different hepatic stromal cells were used to predict context-specific activity of metabolic networks reflecting the metabolic state of the cell cultures in each condition. After checking the consistency of the template model [44] a mixed-integer optimization problem was solved to identify reactions which were part of flux distributions supported by highly expressed genes while avoiding fluxes through reactions catalyzed by lowly expressed genes [45]. For each cell type and each coculture condition an individual metabolic model was derived. The simulation predicts activities for all metabolic reactions in mmol/h. Activity values higher than zero indicate a predicted activity. Values were considered to be low, when the predicted activity was close to zero. Different levels of activity are quantitative [mmol/h] and are therefore comparable.

2.15. Simulation of metabolism of HSCs, HMFs, and PDECs

Coculture condition-specific models were used for computational growth experiments in line with the original experimental setup using BacArena version 1.7 [46]. Nutrient availability was determined on literature-based information on medium composition used in the respective cocultures (see 2.4). For each experimental replicate, three computational replicates were performed. The BacArena grid size was set to 50 × 50 with initially 50 cells per cell type and a simulation time of 8 h per replicate.

2.16. Statistical analysis

Relationships between data from immunohistochemical stainings of pancreatic tissues were categorized and compared between groups by Fisher's exact test using SPSS 17.0 (IBM, Ehningen, Germany). Statistical analysis of *in vitro* data was performed using SigmaPlot Software 12 (Systat Software GmbH, Erkrath, Germany). The Shapiro-Wilk test was used to test for normal distribution. Normally distributed data were analyzed by two-tailed *t*-test (if not otherwise indicated). Non-parametric data were analyzed by Mann-Whitney rank sum test. Statistical analysis of exchanges and reaction activity in computational models included the readout of the simulation which was substance concentrations, produced and consumed substances and reaction activity over time for each computational replicate. Significant differences between cultures of PDECs cocultured with HSC or HMF were checked using a linear mixed-effect model. Reaction activity was considered as dependent variable and culture as fixed independent factor.

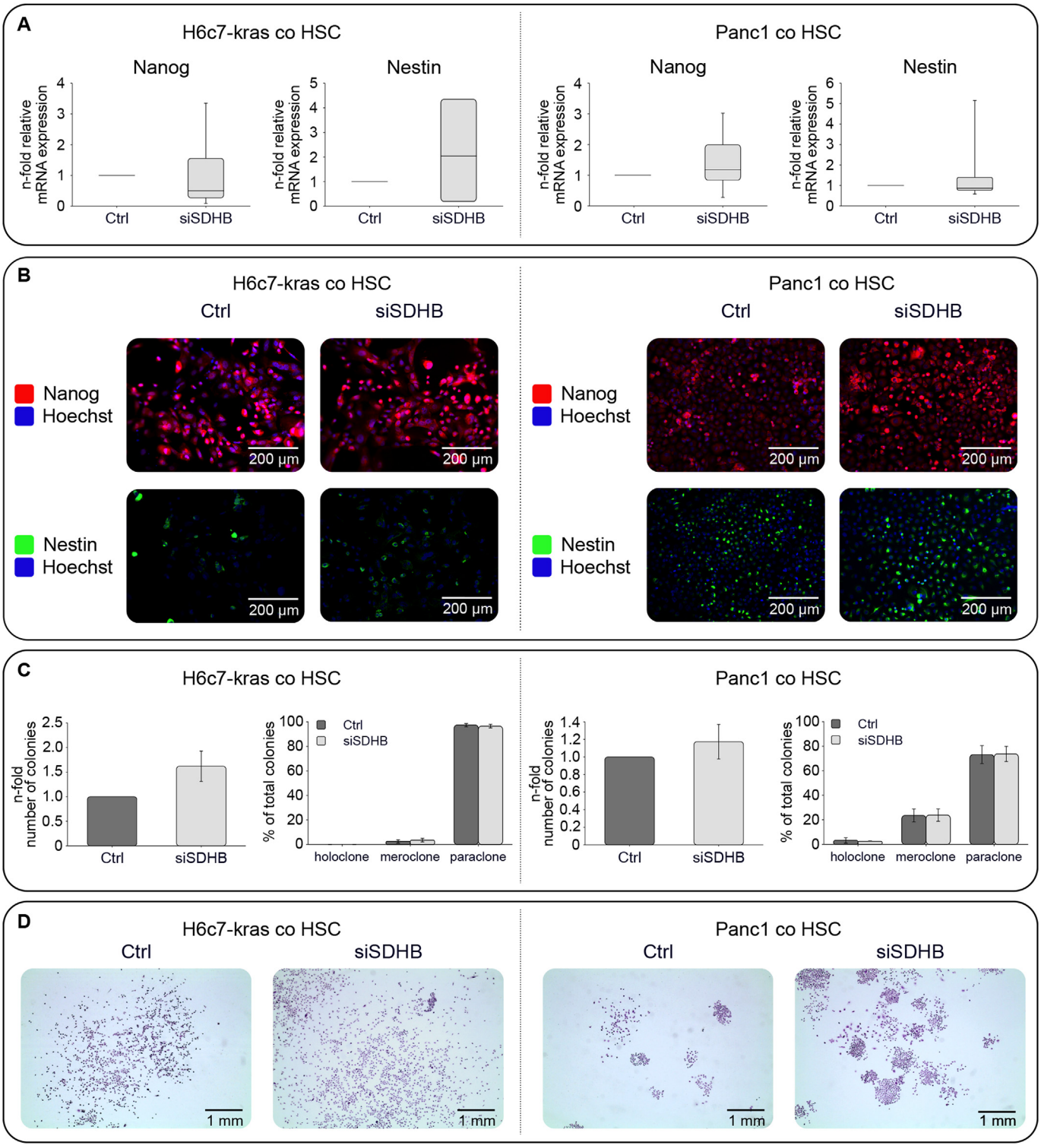

Fig. 4. SDHB has minor impact on stemness properties of PDECs. H6c7-kras or Panc1 cells were transfected with control siRNA (Ctrl) or SDHB siRNA (siSDHB), respectively. After one day, indirect coculture (co) with HSC was started and PDECs were analyzed after five days. **(A)** Expression of Nanog and Nestin was determined by RT-qPCR and normalized to the house keeping gene GAPDH. Data are presented as n-fold mRNA expression with control siRNA transfected PDECs set as 1. Bars display median ± quartiles ($Q_{0.75}$ as upper, $Q_{0.25}$ as lower deviation) of at least 3 independent experiments. (**B**) Shown are representative *in vitro* immunofluorescence stainings of Nanog and Nestin. Hoechst was used as nuclei stain in H6c7-kras and Panc1 cells. (**C**) Number of colonies of PDECs transfected with control siRNA being set as 1 and different colony forms (holoclone, meroclone, paraclone) presented as percentage of total colonies are shown. Bars show mean ± SEM of at least 4 independent experiments. (**D**) Representative images of PDEC colony formation are shown.

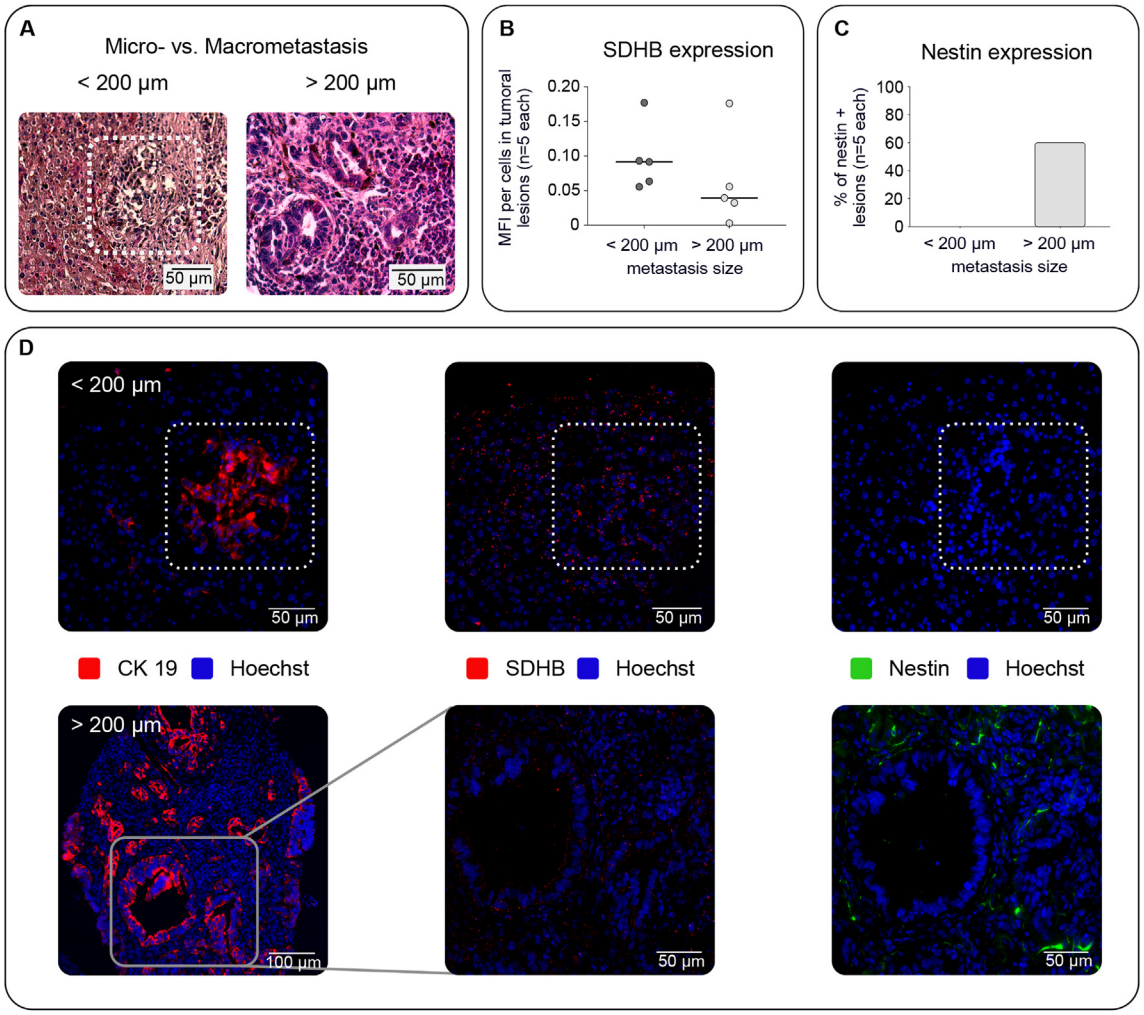

Fig. 5. Macrometastases in the liver of PDAC bearing KPC mice are characterized by a low SDHB expression but elevated Nestin expression compared to micrometastases. Liver sections of mice harboring endogenous advanced PDAC (n = 5) were examined for the presence of micrometastases (lesion diameter ≤ 200 µm) and macrometastases (lesion diameter > 200 µm) by (A) HE-staining and (B_D) staining of Cytokeratin-19 (CK-19) to detect the tumoral lesions, (**B** + **D**) SDHB and (**C** + **D**) Nestin. Hoechst was used as nuclei stain. **A**) Representative images of micro- and macrometastases in HE-stainings are shown. **B)** Scoring of SDHB expression presented as median fluorescence intensity (MFI)/cell and **C)** Scoring of Nestin expression presented as number of Nestin + lesions. **D)** Representative images of single stainings performed in serial sections from a micrometastasis (top, dotted line) and a macrometastasis (bottom) are shown.

Simulation times as well as replicates were considered as random effects. The model was fitted using the R package lme4 [47] and p-values were calculated by likelihood ratio test against a control model without the fixed effect of interest (i.e. HSC vs. HMF-culture). Screening of scientific literature for gene-cancer associations was performed using the semedico search engine [48]. *P*-values < 0.05, < 0.01 or < 0.001 were regarded as statistically significant and are indicated with asterisks (*, ** or *** respectively).

3. Results

3.1. Cell growth and metabolic status of H6c7-kras and Panc1 cells are dependent on the hepatic microenvironment

The PDEC lines H6c7-kras and Panc1 exhibit a dormant cell status (flattened morphology, Ki67-, SABG+, high pp38/pErk ratio) in the presence of HSC compared to coculture with HMF [8]. In contrast, HMF coculture promotes reversal of this quiescent phenotype and proliferation of PDECs underscoring the impact of the hepatic microenvironment on growth behavior of disseminated PDECs and metastatic outgrowth in the liver [8]. To investigate whether these phenotypic and functional alterations are associated with metabolic reprogramming, the metabolic status of benign (H6c7-pBp), premalignant (H6c7-kras) and malignant (Panc1) PDECs in response to different hepatic stromal cells was analyzed by determining the expression of key enzymes of glycolysis, PPP and OXPHOS. No differences with respect to Lactate dehydrogenases A and B (LDHA/LDHB), Transaldolase (TALDO) and 6-Phosphogluconate dehydrogenase (PGD) were detected in the three cell lines when cocultered with either HSC or HMF (Fig. 1A). Transketolase (TKT) was only less expressed in H6c7-pBp cells under HMF coculture but not affected in the other cell lines. G6PD was slightly higher expressed in PDECs under HMF-coculture. Expression of Monocarboxylate Transporter 4 (MCT4) being indicative for glycolysis was not altered by the different coculture conditions. Most strikingly, premalignant and malignant PDEC lines showed a clearly elevated SDHB expression in the presence of HSC compared to HMF-coculture (Fig. 1A + B). Thus, low proliferative activity of premalignant and malignant PDECs seemed to be associated with enhanced SDHB expression under HSC-coculture. Of note, in line with their malignant phenotype monocultured Panc1 cells were characterized by a low SDHB expression compared to premalignant H6c7-kras and benign H6c7-pBp cells (Supplementary Fig. 1). To analyze whether stromal cell-mediated differences in SDHB expression are indicative for an altered OXPHOS and mitochondrial activity, oxygen consumption rate (OCR) in differentially cocultured

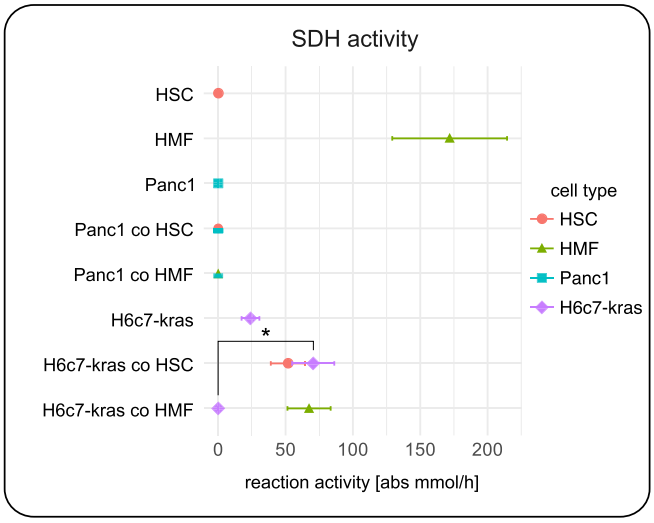

Fig. 6. *In silico* predicted SDH activity in mono- and cocultured PDECs and hepatic stromal cells. Predicted reaction fluxes of SDH in H6c7-kras and Panc1 cells as well as HSC and HMF, each cultured under mono- and coculture conditions are shown. Data are expressed as reaction activity (absolute mmol/h). Simulation was performed in triplicates of three independent experiments. * = $p < 0.05$.

H6c7-kras cells was measured. In line with the elevated SDHB expression, HSC-cocultured H6c7-kras cells exhibited a significantly higher basal OCR and responded much stronger to FCCP treatment compared to cells after HMF-coculture, the latter showing a significantly higher reserve respiratory capacity (Fig. 2A+B). Together with our previous findings [8] these data suggest that PDECs when exposed to HSCs are characterized by elevated SDHB expression along with an oxidative phenotype (Fig. 2A + B) both being associated with a quiescent cell status. In contrast, HMF-cocultured PDECs exhibited lower SDHB expression and a glycolytic phenotype (Fig. 2C) along with elevated cell growth.

3.2. Downregulation of SDHB expression in HSC-cocultured H6c7-kras and Panc1 cells leads to enhanced cell growth

In order to investigate whether enhanced SDHB expression is responsible for HSC-mediated alterations in PDECs, SDHB expression was transiently downregulated by siRNA treatment before PDECs were cocultured in the presence of HSC. Along with the reduced SDHB expression (Fig. 3A), both, basal OXPHOS and reserve respiratory capacity, were clearly diminished leading to a shift from an oxidative to a more glycolytic phenotype (Supplementary Fig. 2A + B) comparable to that acquired upon HMF-coculture (Fig. 2C). Furthermore, SDHB knockdown significantly enhanced cell growth of both cell lines increasing the numbers of vital cells 1.78-fold and 1.97-fold in HSC-cocultured H6c7-kras and Panc1 cells, respectively (Fig. 3B), being similar to vital cell numbers observed after HMF-coculture (data not shown). Moreover, the proportion of SABG + cells – indicative for a quiescent phenotype - was reduced (Fig. 3C), while the proportion of proliferating Ki67 + cells was enhanced (Fig. 3D), both effects being more pronounced in H6c7-kras than Panc1 cells. These data indicate that HSCs promote an enhanced SDHB expression along with an oxidative phenotype in PDECs conferring a quiescent cell state.

3.3. Downregulation of HSC-mediated SDHB expression in H6c7-kras and Panc1 cells increases CSC-properties

It has been recently shown that CSC-properties of PDECs are maintained and promoted by the hepatic microenvironment [18]. To investigate whether SDHB expression level not only affects cell growth but also CSC-properties in PDECs, HSC-cocultured H6c7-kras and Panc1 cells either transfected with control siRNA or SDHB siRNA were characterized with respect to expression of the CSC-markers Nanog and Nestin as well as self-renewal capacity. While no clear effect could be observed on Nanog RNA and protein levels, Nestin expression was enhanced after SDHB knockdown, being more pronounced on protein level and in H6c7-kras cells compared to Panc1 cells (Fig. 4A + B). In line with the increased Nestin expression, SDHB suppression elevated self-renewal capacity in both PDEC lines being more pronounced in H6c7-kras cells than Panc1 cells leading to formation of more and larger colonies (Fig. 4C + D). In detail, the number of H6c7-kras colonies was increased 1.62-fold after SDHB knockdown compared to control transfected cells. However, no alterations in the formation of the different colony morphologies (holo-, mero- and paraclones) were noticed in either cell line (Fig. 4C). These data indicate that the oxidative metabolic phenotype of PDECs acquired under HSC coculture, being sustained and characterized by SDHB expression, is associated with an alteration in proliferative activity and CSC-properties.

3.4. Liver micrometastases of PDAC bearing KPC mice are characterized by a higher SDHB expression and lower Nestin expression than macrometastases

Liver micrometastases (< 200 µm) of tumor bearing KPC mice are characterized by a low proliferative activity and surrounded by an unobtrusive, HSCs containing liver micromilieu. In contrast,

Table 1
Significantly different reaction activities of distinct metabolic subsystems in H6c7-kras cells under HSC- and HMF-coculture. Significant differences between reaction activities are shown for H6c7-kras cocultured (co) with HSC or HMF as mean log2 fold changes. Positive values indicate that H6c7-kras co HMF reaction activities are higher compared to H6c7-kras co HSC and negative values vice versa. Simulation was performed in triplicates of three independent experiments.

Subsystem	reaction	name	mean log2 fold change	p-value bonferroni corrected
Citric acid cycle	ACONT	aconitase hydratase	4,75	5.276E-07
	ACONTm	aconitate hydratase, mitochondrial	3,93	5.452E-07
	ICDHyrm	Isocitrate dehydrogenase (NADP+), mitochondrial	3,60	1.202E-07
	SUCD1m	succinate dehydrogenase, mitochondrial	−25,0	0.015
Glycolysis/gluconeogenesis	ENO	enolase	2,78	4.028E-05
	FBA	fructose-bisphosphate aldolase	3,75	0.04
	GAPD	glyceraldehyde-3-phosphate dehydrogenase	2,75	8.330E-05
	PFK	phosphofructokinase	3,75	0.04
	PGK	phosphoglycerate kinase	2,75	8.330E-05
	PGM	phosphoglycerate mutase	2,78	4.028E-05
	PYK	pyruvate kinase	3,02	3.216E-05
	TPI	triose-phosphate isomerase	3,26	0.003
Pentose phosphate pathway	r0407	Sedoheptulose 1,7-bisphosphate D-glyceraldehyde-3-phosphate-lyase Carbon fixation	3,26	0.023

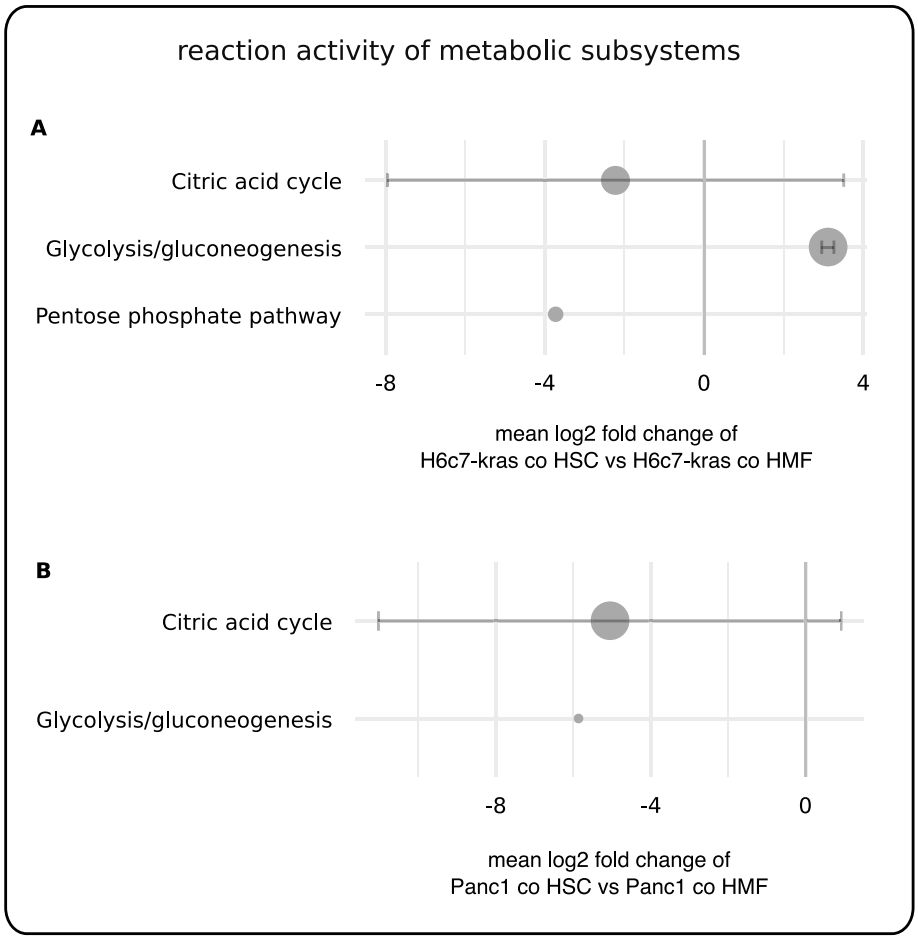

Fig. 7. ***In silico*** **modeling indicates that metabolic subsystems significantly differ in H6c7-kras and Panc1 cells under HSC- and HMF-coculture.** Significant differences between reaction activities are shown for **A)** H6c7-kras cells and **B)** Panc1 cells cocultured (co) with HSC or HMF as mean log2 fold changes. Positive values indicate that H6c7-kras/Panc1 co HMF reaction activities are higher compared to H6c7-kras/Panc1 co HSC and negative values vice versa. Reactions are summarized in metabolic subsystems citric acid cycle, glycolysis/gluconeogenesis and pentose phosphate pathway. For each subsystem standard deviation is shown and relative point size indicates how many reactions with significant difference have been detected in each subsystem. Simulation was performed in triplicates of three independent experiments.

Table 2
Significantly different reaction activities of distinct metabolic subsystems in Panc1 cells under HSC- and HMF-coculture. Significant differences between reaction activities are shown for Panc1 cells cocultured (co) with HSC or HMF as mean log2 fold changes. Positive values indicate that Panc1 co HMF reaction activities are higher compared to Panc1 co HSC and negative values vice versa. Simulation was performed in triplicates of three independent experiments.

Subsystem	reaction	name	mean log2 fold change	p-value bonferroni corrected
Citric acid cycle	CSm	citrate synthase, mitochondrial	5,55	0.049
	MDHm	malate dehydrogenase, mitochondrial	−1,94	0.002
	r0384	2-oxoglutarate:[dihydrolipoyllysine-residue succinyltransferase]-lipoyllysine 2-oxidoreductase (decarboxylating, acceptor-succinylating)	−28,27	1.06E-09
	SUCOAS1m	Succinate–CoA ligase (GDP-forming), mitochondrial	−2,10	1.618E-05
	SUCOASm	Succinate–CoA ligase (GDP-forming), mitochondrial	1,50	0.005
Glycolysis/gluconeogenesis	PYK	pyruvate kinase	−5,86	5.431E-10

macrometastases (> 200 μm) exhibited a higher proportion of proliferating Ki67 + tumor cells being located in an HMFs enriched microenvironment further supporting the view that HSCs promote a dormant phenotype in disseminated PDAC cells [8]. To analyze whether the *in vitro* identified association of reduced cell growth of PDAC cells and enhanced SDHB expression in the presence of HSCs also applies *in situ,* consecutive liver sections of KPC mice containing micro- and macrometastases (Fig. 5A) were analyzed for SDHB expression. In accordance with our findings of an elevated SDHB expression in PDECS under HSC-coculture compared to HMF-coculture (Fig. 1), micrometastases exhibited stronger SDHB expression compared to macrometastases (Fig. 5B + D). Furthermore, micrometastases exhibited low to no Nestin expression, while considerable Nestin expression was observed in 3/5 macrometastases (Fig. 5C + D) supporting our *in vitro* findings of a CSC-suppressing role of SDHB in PDAC cells.

3.5. The hepatic microenvironment influences in silico SDH activity

To gain further insight into metabolic interactions of PDECs with hepatic stromal cells, RNA-sequencing and differential gene expression analysis were performed of mono- and cocultured H6c7-kras and Panc1 cells as well as mono- and cocultured HSC and HMF. Through mapping of the expression data on a generic model of cellular metabolism and subsequent simulation of the individual models in mono- and coculture, metabolic activity was investigated in the individual cell types. In line with the elevated SDHB expression (Fig. 1) and OCR (Fig. 2) experimentally determined under these conditions, *in silico* data indicate that predominantly H6c7-kras cells acquired a significantly higher SDH activity in the presence of HSC compared to the presence of HMF (Fig. 6). Thus, predicted activity of H6c7-kras cells was 0 when grown together with HMF cells indicating that these cells exhibited no SDH activity under these conditions. However, predicted activity was > 0

when cells were grown together with HSC pointing to a higher SDH activity which is in line with our experimental data.

Moreover, HSC exhibited no considerable flux through SDH in monoculture, whereas SDH activity was enhanced under coculture with H6c7-kras cells. In contrast, cocultured HMF showed a lower SDH activity compared to monocultured HMF. For Panc1 cells, no change in SDH activity could be predicted. Overall, these data suggest that an uninflamed hepatic microenvironment promotes SDH activity predominantly in premalignant PDECs with HSC being also characterized by an elevated metabolic flux through SDH.

3.6. Activity in metabolic subsystems significantly differs in H6c7-kras and Panc1 cells under HSC- and HMF-coculture

Next, we used computational growth experiments to simulate the metabolism of each cellular population under the respective culture conditions. Computational modeling predicted 13 significantly different reaction activities in the metabolic subsystems citric acid cycle, glycolysis and PPP in H6c7-kras cells cultured in the presence of HSC compared to HMF-coculture (Table 1, Fig. 7A). The most significant change was predicted in the activity of SDH in HSC-cocultured H6c7-kras cells compared to HMF-coculture (−25 log2 fold change in reaction activity). Moreover, H6c7-kras cells cocultured with HMF were predicted to be significantly more glycolytic (Table 1, positive fold change in reactions being involved in glycolysis) than after HSC-coculture confirming our experimental data (Fig. 2). Again, in line with the coculture data (Fig. 1), significantly altered reaction activities in Panc1 cells in dependence of different coculture conditions were predicted, too, albeit less pronounced than in H6c7-kras cells (Table 2, Fig. 7B). Six altered reaction activities in citric acid cycle and glycolysis were predicted with 2-oxoglutarate:[dihydrolipoyllysine-residue succinyltransferase]-lipoyllysine 2-oxidoreductase (decarboxylating, acceptor-succinylating) showing the strongest fold change in HSC-cocultured Panc1 cells compared to HMF-coculture (−28 log2 fold change in reaction activity). Supporting our experimental data, *in silico* modeling predicted changes in the metabolism of PDECs in response to different hepatic stromal cells and that the changes in the metabolism of premalignant H6c7-kras cells seemed to be more pronounced than those of malignant Panc1 cells.

4. Discussion

The liver is the primary target for metastasis formation in PDAC and liver metastases are a major burden for PDAC patients essentially limiting their overall survival [49]. Mechanistically, there is increasing evidence for the prometastatic character of an inflamed liver microenvironment [4–6]. Therein, HSCs play a pivotal role in supporting colonization and tumor cell growth once they are activated and transdifferentiated into HMFs by inflammatory signals. Even though an altered metabolism is a hallmark of cancer, the influence of HSCs compared to HMFs on the metabolism of disseminated PDECs is unknown.

To get further insight into these interactions we used a well-established indirect coculture system with HSCs and HMFs, respectively, to model the hepatic microenvironment under different inflammatory conditions and H6c7-kras and Panc1 being two PDEC lines differing with respect to PDAC-associated mutations. Using this model along with two different *in vivo* PDAC mouse models we demonstrated that HSCs promote a dormant phenotype in PDECs while the presence of HMFs fosters the reversal of this quiescent phenotype and leads to a proliferation boost of PDECs [8]. Extending these findings, the present study demonstrates that premalignant and malignant but not benign PDECs showed a clearly enhanced expression of SDHB in the presence of HSCs compared to HMFs being more pronounced in premalignant H6c7-kras cells than in Panc1 cells. Consistently, a significantly increased OXPHOS was determined in HSC-cocultured H6c7-kras cells. One explanation for the stronger effects in the metabolic adaptation of H6c7-kras cells in response to the hepatic micromilieu could be that these cells harbor fewer genetic alterations than malignant Panc1 cells which determine the cell's fate and behavior. Thus, these premalignant cells still exhibit a higher plasticity implying also metabolic adaptation to the environmental conditions. Supporting our findings, a marked and lasting decrease in SDH-activity in premalignant hepatic lesions could be associated with a high risk for progression into hepatocellular carcinoma [50] while OXPHOS was decreased in prostate and PDAC cells when exposed to tumor-associated fibroblast-derived exosomes [51].

Several studies suggest a role of SDHB as a tumor suppressor in different tumor entities and a role as oncometabolite for its substrate succinate [52–55]. Accordingly, siRNA-mediated SDHB knockdown in HSC-cocultured PDECs led to a reduced SDHB expression along with a significantly reduced OXPHOS compared to control transfected cells. Furthermore, SDHB knockdown enhanced cell growth of PDECs and diminished signs of quiescence under HSC-coculture leading to comparable cell growth as after HMF-coculture without SDHB knockdown (data not shown). Intriguingly, the above mentioned studies [53–55] also highlight an inverse correlation between SDHB expression and cancer stemness such as self-renewal capacity. This is in line with our observation that CSC-properties in HSC-cocultured PDECs increased after SDHB knockdown predominantly exemplified by elevated colony formation. Further supporting a metastasis-suppressing role for HSC-associated SDHB expression, liver micrometastases of tumor bearing KPC mice were characterized by a prominent SDHB expression and almost undetectable Nestin expression while macrometastases exhibited a converse expression profile. These data are also consistent with the observation that Nestin knockdown significantly reduced formation of liver metastases in a murine PDAC model [17].

However, the relation between SDH and OXPHOS activity and CSC-properties particularly in the metastatic context remains still poorly understood. Two studies described a high dependency on OXPHOS in pancreatic CSCs because inhibiting OXPHOS depleted the CSC pool and impeded outgrowth of tumor spheres [56,57]. Explanations for the discrepant findings to our study might be: i) selective inhibition of the tumor suppressor SDHB instead of general OXPHOS suppression differentially impacts CSC-properties and tumor outgrowth or ii) different CSC subsets as described for normal stem cells may exist (slow-cycling versus fast-cycling stem cell populations [58]) which are differentially dependent on SDH activity and OXPHOS.

To gain further insight into the metabolic adaptation process of PDECs to the hepatic microenvironment, RNA-sequencing and computational modeling was used to simulate the metabolism of each cellular population under different stromal conditions. The results supported our experimental data by predicting a more oxidative phenotype under HSC-coculture with elevated SDH activity and a more glycolytic phenotype in the presence of HMF. On the global metabolic scale, metabolic modeling revealed not only changes in glycolytic and TCA cycle activity, but also a pronounced change in the activity of several other pathways that have been linked to cancer growth in a coculture-dependent fashion (data not shown). Additionally, all seven significantly changed reaction steps in glycolysis, predicted to be more active in HMF-cocultured cells, have already been associated with cancer. Especially phosphofructokinase was shown to be highly expressed in liver tumors [59] as well as enolase [60], phosphoglycerate kinase [61], glyceraldehyde-3-phosphate dehydrogenase [62] promoting tumor growth and metastasis. Overall, these results support a global remodeling of a cancer promoting metabolism in response to the pro-inflammatory environment promoted by HMF.

Our previous studies [8] and the present study suggest the following role of the hepatic microenvironment in metastases formation in PDAC: A physiological (non-inflamed) hepatic micromilieu, showing significantly higher amounts of HSCs than HMFs, leads to elevated SDHB expression and an oxidative metabolic phenotype in disseminated PDECs thereby promoting a dormant stage. It has still to be elucidated whether elevated SDHB expression is the cause or consequence of the

metabolic adaption of PDECs to the liver stroma. Concomitantly, CSC-properties are maintained but controlled by the metabolic phenotype of PDECs that seems to be mechanistically linked to SDHB expression levels, thus underscoring a role of a physiological liver micromilieu and SDHB as a tumor suppressor. Aging or exposure to certain life style factors such as alcohol leads to transdifferentiation of HSCs into HMFs and thereby to a (smouldering) liver inflammation. As a consequence, this inflammatory switch promotes the downregulation of the tumor suppressor SDHB and the acquisition of a glycolytic phenotype in PDECs thereby fostering proliferation, self-renewal abilities and outgrowth of visible metastases.

Funding

Financial support by the German Cancer Aid (S.Se.), the Deutsche Forschungsgemeinschaft (H.S. and G.M.), the excellence cluster “Inflammation at Interfaces” (C.K.) and the UKSH Förderstiftung (S.Se.) is acknowledged.

Conflict of interest disclosure

The authors disclose no conflict of interest.

Acknowledgements

The authors thank Dagmar Leisner for excellent technical assistance.

Appendix A. Supplementary data

Supplementary data to this article can be found online at https://doi.org/10.1016/j.canlet.2019.03.039.

References

[1] M. Malvezzi, G. Carioli, P. Bertuccio, P. Boffetta, F. Levi, C. La Vecchia, E. Negri, European cancer mortality predictions for the year 2018 with focus on colorectal cancer, Ann. Oncol. 29 (2018) 1016–1022, https://doi.org/10.1093/annonc/mdy033.

[2] V.P. Groot, N. Rezaee, W. Wu, J.L. Cameron, E.K. Fishman, R.H. Hruban, M.J. Weiss, L. Zheng, C.L. Wolfgang, J. He, Patterns, timing, and predictors of recurrence following pancreatectomy for pancreatic ductal adenocarcinoma, Ann. Surg. 267 (2018) 936–945, https://doi.org/10.1097/SLA.0000000000002234.

[3] A.D. Rhim, E.T. Mirek, N.M. Aiello, A. Maitra, J.M. Bailey, F. McAllister, M. Reichert, G.L. Beatty, A.K. Rustgi, R.H. Vonderheide, S.D. Leach, B.Z. Stanger, EMT and dissemination precede pancreatic tumor formation, Cell 148 (2012) 349–361, https://doi.org/10.1016/j.cell.2011.11.025.

[4] S.R. Nielsen, V. Quaranta, A. Linford, P. Emeagi, C. Rainer, A. Santos, L. Ireland, T. Sakai, K. Sakai, Y.S. Kim, D. Engle, F. Campbell, D. Palmer, J.H. Ko, D.A. Tuveson, E. Hirsch, A. Mielgo, M.C. Schmid, Macrophage-secreted granulin supports pancreatic cancer metastasis by inducing liver fibrosis, Nat. Cell Biol. 18 (2016) 549–560, https://doi.org/10.1038/ncb3340.

[5] B. Costa-Silva, N.M. Aiello, A.J. Ocean, S. Singh, H. Zhang, B.K. Thakur, A. Becker, A. Hoshino, M.T. Mark, H. Molina, J. Xiang, T. Zhang, T.M. Theilen, G. Garcia-Santos, C. Williams, Y. Ararso, Y. Huang, G. Rodrigues, T.L. Shen, K.J. Labori, I.M. Lothe, E.H. Kure, J. Hernandez, A. Doussot, S.H. Ebbesen, P.M. Grandgenett, M.A. Hollingsworth, M. Jain, K. Mallya, S.K. Batra, W.R. Jarnagin, R.E. Schwartz, I. Matei, H. Peinado, B.Z. Stanger, J. Bromberg, D. Lyden, Pancreatic cancer exosomes initiate pre-metastatic niche formation in the liver, Nat. Cell Biol. 17 (2015) 816–826, https://doi.org/10.1038/ncb3169.

[6] B. Grunwald, V. Harant, S. Schaten, M. Fruhschutz, R. Spallek, B. Hochst, K. Stutzer, S. Berchtold, M. Erkan, O. Prokopchuk, M. Martignoni, I. Esposito, M. Heikenwalder, A. Gupta, J. Siveke, P. Saftig, P. Knolle, D. Wohlleber, A. Kruger, Pancreatic premalignant lesions secrete tissue inhibitor of metalloproteinases-1, which activates hepatic stellate cells via CD63 signaling to create a premetastatic niche in the liver, Gastroenterology 151 (2016) 1011–1024, https://doi.org/10.1053/j.gastro.2016.07.043 e1017.

[7] P. Kocabayoglu, S.L. Friedman, Cellular basis of hepatic fibrosis and its role in inflammation and cancer, Front. Biosci. (Schol Ed) 5 (2013) 217–230.

[8] L. Lenk, M. Pein, O. Will, B. Gomez, F. Viol, C. Hauser, J.-H. Egberts, J.-P. Gundlach, O. Helm, S. Tiwari, R. Weiskirchen, S. Rose-John, C. Röcken, W. Mikulits, P. Wenzel, G. Schneider, D. Saur, H. Schäfer, S. Sebens, The hepatic microenvironment essentially determines tumor cell dormancy and metastatic outgrowth of pancreatic ductal adenocarcinoma, OncoImmunology (2017) e1368603, , https://doi.org/10.1080/2162402X.2017.1368603.

[9] M.L. O'Connor, D. Xiang, S. Shigdar, J. Macdonald, Y. Li, T. Wang, C. Pu, Z. Wang, L. Qiao, W. Duan, Cancer stem cells: a contentious hypothesis now moving forward, Cancer Lett. 344 (2014) 180–187, https://doi.org/10.1016/j.canlet.2013.11.012.

[10] J.A. Magee, E. Piskounova, S.J. Morrison, Cancer stem cells: impact, heterogeneity, and uncertainty, Cancer Cell 21 (2012) 283–296, https://doi.org/10.1016/j.ccr.2012.03.003.

[11] H.X. Zhan, J.W. Xu, D. Wu, T.P. Zhang, S.Y. Hu, Pancreatic cancer stem cells: new insight into a stubborn disease, Cancer Lett. 357 (2015) 429–437, https://doi.org/10.1016/j.canlet.2014.12.004.

[12] C. Li, D.G. Heidt, P. Dalerba, C.F. Burant, L. Zhang, V. Adsay, M. Wicha, M.F. Clarke, D.M. Simeone, Identification of pancreatic cancer stem cells, Cancer Res. 67 (2007) 1030–1037, https://doi.org/10.1158/0008-5472.CAN-06-2030.

[13] P.C. Hermann, S.L. Huber, T. Herrler, A. Aicher, J.W. Ellwart, M. Guba, C.J. Bruns, C. Heeschen, Distinct populations of cancer stem cells determine tumor growth and metastatic activity in human pancreatic cancer, Cell Stem Cell 1 (2007) 313–323, https://doi.org/10.1016/j.stem.2007.06.002.

[14] R.J. Vanner, M. Remke, M. Gallo, H.J. Selvadurai, F. Coutinho, L. Lee, M. Kushida, R. Head, S. Morrissy, X. Zhu, T. Aviv, V. Voisin, I.D. Clarke, Y. Li, A.J. Mungall, R.A. Moore, Y. Ma, S.J. Jones, M.A. Marra, D. Malkin, P.A. Northcott, M. Kool, S.M. Pfister, G. Bader, K. Hochedlinger, A. Korshunov, M.D. Taylor, P.B. Dirks, Quiescent sox2(+) cells drive hierarchical growth and relapse in sonic hedgehog subgroup medulloblastoma, Cancer Cell 26 (2014) 33–47, https://doi.org/10.1016/j.ccr.2014.05.005.

[15] H.T. Su, C.C. Weng, P.J. Hsiao, L.H. Chen, T.L. Kuo, Y.W. Chen, K.K. Kuo, K.H. Cheng, Stem cell marker nestin is critical for TGF-beta1-mediated tumor progression in pancreatic cancer, Mol. Canc. Res. 11 (2013) 768–779, https://doi.org/10.1158/1541-7786.MCR-12-0511.

[16] Y. Matsuda, H. Yoshimura, J. Ueda, Z. Naito, M. Korc, T. Ishiwata, Nestin delineates pancreatic cancer stem cells in metastatic foci of NOD/Shi-scid IL2Rgamma(null) (NOG) mice, Am. J. Pathol. 184 (2014) 674–685, https://doi.org/10.1016/j.ajpath.2013.11.014.

[17] Y. Matsuda, T. Ishiwata, H. Yoshimura, S. Yamashita, T. Ushijima, T. Arai, Systemic administration of small interfering RNA targeting human nestin inhibits pancreatic cancer cell proliferation and metastasis, Pancreas 45 (2016) 93–100, https://doi.org/10.1097/MPA.0000000000000427.

[18] H. Knaack, L. Lenk, L.-M. Philipp, L. Miarka, S. Rahn, F. Viol, C. Hauser, J.H. Egberts, J.-P. Gundlach, O. Will, S. Tiwari, W. Mikulits, U. Schumacher, J.G. Hengstler, S. Sebens, Liver metastasis of pancreatic cancer: the hepatic microenvironment impacts differentiation and self-renewal capacity of pancreatic ductal epithelial cells, Oncotarget 9 (2018) 31771–31786, https://doi.org/10.18632/oncotarget.25884.

[19] D. Hanahan, R.A. Weinberg, Hallmarks of cancer: the next generation, Cell 144 (2011) 646–674, https://doi.org/10.1016/j.cell.2011.02.013.

[20] N. Hay, Reprogramming glucose metabolism in cancer: can it be exploited for cancer therapy? Nat. Rev. Canc. 16 (2016) 635–649, https://doi.org/10.1038/nrc.2016.77.

[21] O. Warburg, On the origin of cancer cells, Science 123 (1956) 309–314, https://doi.org/10.1126/science.123.3191.309.

[22] G. Lucarelli, V. Galleggiante, M. Rutigliano, F. Sanguedolce, S. Cagiano, P. Bufo, G. Lastilla, E. Maiorano, D. Ribatti, A. Giglio, G. Serino, A. Vavallo, C. Bettocchi, F.P. Selvaggi, M. Battaglia, P. Ditonno, Metabolomic profile of glycolysis and the pentose phosphate pathway identifies the central role of glucose-6-phosphate dehydrogenase in clear cell-renal cell carcinoma, Oncotarget 6 (2015) 13371–13386, https://doi.org/10.18632/oncotarget.3823.

[23] W.H. Koppenol, P.L. Bounds, C.V. Dang, Otto Warburg's contributions to current concepts of cancer metabolism, Nat. Rev. Canc. 11 (2011) 325–337, https://doi.org/10.1038/nrc3038.

[24] X. Wang, X. Li, X. Zhang, R. Fan, H. Gu, Y. Shi, H. Liu, Glucose-6-phosphate dehydrogenase expression is correlated with poor clinical prognosis in esophageal squamous cell carcinoma, Eur. J. Surg. Oncol. 41 (2015) 1293–1299, https://doi.org/10.1016/j.ejso.2015.08.155.

[25] H. Pu, Q. Zhang, C. Zhao, L. Shi, Y. Wang, J. Wang, M. Zhang, Overexpression of G6PD is associated with high risks of recurrent metastasis and poor progression-free survival in primary breast carcinoma, World J. Surg. Oncol. 13 (2015) 323, https://doi.org/10.1186/s12957-015-0733-0.

[26] D. Whitaker-Menezes, U.E. Martinez-Outschoorn, Z. Lin, A. Ertel, N. Flomenberg, A.K. Witkiewicz, R. Birbe, A. Howell, S. Pavlides, R. Gandara, R.G. Pestell, F. Sotgia, N.J. Philp, M.P. Lisanti, Evidence for a stromal-epithelial “lactate shuttle” in human tumors, Cell Cycle 10 (2011) 1772–1783, https://doi.org/10.4161/cc.10.11.15659.

[27] C. Guido, D. Whitaker-Menezes, C. Capparelli, R. Balliet, Z. Lin, R.G. Pestell, A. Howell, S. Aquila, S. Ando, U. Martinez-Outschoorn, F. Sotgia, M.P. Lisanti, Metabolic reprogramming of cancer-associated fibroblasts by TGF-beta drives tumor growth: connecting TGF-beta signaling with "Warburg-like" cancer metabolism and L-lactate production, Cell Cycle 11 (2012) 3019–3035, https://doi.org/10.4161/cc.21384.

[28] J.M. Curry, M. Tuluc, D. Whitaker-Menezes, J.A. Ames, A. Anantharaman, A. Butera, B. Leiby, D.M. Cognetti, F. Sotgia, M.P. Lisanti, U.E. Martinez-Outschoorn, Cancer metabolism, stemness and tumor recurrence: MCT1 and MCT4 are functional biomarkers of metabolic symbiosis in head and neck cancer, Cell Cycle 12 (2013) 1371–1384, https://doi.org/10.4161/cc.24092.

[29] C. Carmona-Fontaine, V. Bucci, L. Akkari, M. Deforet, J.A. Joyce, J.B. Xavier, Emergence of spatial structure in the tumor microenvironment due to the Warburg effect, Proc. Natl. Acad. Sci. U. S. A 110 (2013) 19402–19407, https://doi.org/10.1073/pnas.1311939110.

[30] T. Valencia, J.Y. Kim, S. Abu-Baker, J. Moscat-Pardos, C.S. Ahn, M. Reina-Campos, A. Duran, E.A. Castilla, C.M. Metallo, M.T. Diaz-Meco, J. Moscat, Metabolic reprogramming of stromal fibroblasts through p62-mTORC1 signaling promotes

inflammation and tumorigenesis, Cancer Cell 26 (2014) 121–135, https://doi.org/10.1016/j.ccr.2014.05.004.
[31] M. Robertson-Tessi, R.J. Gillies, R.A. Gatenby, A.R. Anderson, Impact of metabolic heterogeneity on tumor growth, invasion, and treatment outcomes, Cancer Res. 75 (2015) 1567–1579, https://doi.org/10.1158/0008-5472.CAN-14-1428.
[32] K. Diehl, L.A. Dinges, O. Helm, N. Ammar, D. Plundrich, A. Arlt, C. Rocken, S. Sebens, H. Schafer, Nuclear factor E2-related factor-2 has a differential impact on MCT1 and MCT4 lactate carrier expression in colonic epithelial cells: a condition favoring metabolic symbiosis between colorectal cancer and stromal cells, Oncogene 37 (2018) 39–51, https://doi.org/10.1038/onc.2017.299.
[33] C. Bardella, P.J. Pollard, I. Tomlinson, SDH mutations in cancer, Biochim. Biophys. Acta 1807 (2011) 1432–1443, https://doi.org/10.1016/j.bbabio.2011.07.003.
[34] A. King, M.A. Selak, E. Gottlieb, Succinate dehydrogenase and fumarate hydratase: linking mitochondrial dysfunction and cancer, Oncogene 25 (2006) 4675–4682, https://doi.org/10.1038/sj.onc.1209594.
[35] C.D. Folmes, P.P. Dzeja, T.J. Nelson, A. Terzic, Metabolic plasticity in stem cell homeostasis and differentiation, Cell Stem Cell 11 (2012) 596–606, https://doi.org/10.1016/j.stem.2012.10.002.
[36] S. Rahn, V. Zimmermann, F. Viol, H. Knaack, K. Stemmer, L. Peters, L. Lenk, H. Ungefroren, D. Saur, H. Schäfer, O. Helm, S. Sebens, Diabetes as risk factor for pancreatic cancer: hyperglycemia promotes epithelial-mesenchymal-transition and stem cell properties in pancreatic ductal epithelial cells, Cancer Lett. 415 (2018) 129–150, https://doi.org/10.1016/j.canlet.2017.12.004.
[37] J. Qian, J. Niu, M. Li, P.J. Chiao, M.S. Tsao, In vitro modeling of human pancreatic duct epithelial cell transformation defines gene expression changes induced by K-ras oncogenic activation in pancreatic carcinogenesis, Cancer Res. 65 (2005) 5045–5053, https://doi.org/10.1158/0008-5472.can-04-3208.
[38] V. Proell, M. Mikula, E. Fuchs, W. Mikulits, The plasticity of p19 ARF null hepatic stellate cells and the dynamics of activation, Biochim. Biophys. Acta 1744 (2005) 76–87, https://doi.org/10.1016/j.bbamcr.2004.12.009.
[39] S. Sebens Muerkoster, V. Werbing, B. Sipos, M.A. Debus, M. Witt, M. Grossmann, D. Leisner, J. Kotteritzsch, H. Kappes, G. Kloppel, P. Altevogt, U.R. Folsch, H. Schafer, Drug-induced expression of the cellular adhesion molecule L1CAM confers anti-apoptotic protection and chemoresistance in pancreatic ductal adenocarcinoma cells, Oncogene 26 (2007) 2759–2768, https://doi.org/10.1038/sj.onc.1210076.
[40] S. Sebens Muerkoster, A.V. Rausch, A. Isberner, J. Minkenberg, E. Blaszczuk, M. Witt, U.R. Folsch, F. Schmitz, H. Schafer, A. Arlt, The apoptosis-inducing effect of gastrin on colorectal cancer cells relates to an increased IEX-1 expression mediating NF-kappa B inhibition, Oncogene 27 (2008) 1122–1134, https://doi.org/10.1038/sj.onc.1210728.
[41] Y. Barrandon, H. Green, Three clonal types of keratinocyte with different capacities for multiplication, Proc. Natl. Acad. Sci. U. S. A 84 (1987) 2302–2306.
[42] C.M. Beaver, A. Ahmed, J.R. Masters, Clonogenicity: holoclones and meroclones contain stem cells, PLoS One 9 (2014) e89834, , https://doi.org/10.1371/journal.pone.0089834.
[43] I. Thiele, N. Swainston, R.M. Fleming, A. Hoppe, S. Sahoo, M.K. Aurich, H. Haraldsdottir, M.L. Mo, O. Rolfsson, M.D. Stobbe, S.G. Thorleifsson, R. Agren, C. Bolling, S. Bordel, A.K. Chavali, P. Dobson, W.B. Dunn, L. Endler, D. Hala, M. Hucka, D. Hull, D. Jameson, N. Jamshidi, J.J. Jonsson, N. Juty, S. Keating, I. Nookaew, N. Le Novere, N. Malys, A. Mazein, J.A. Papin, N.D. Price, E. Selkov Sr., M.I. Sigurdsson, E. Simeonidis, N. Sonnenschein, K. Smallbone, A. Sorokin, J.H. van Beek, D. Weichart, I. Goryanin, J. Nielsen, H.V. Westerhoff, D.B. Kell, P. Mendes, B.O. Palsson, A community-driven global reconstruction of human metabolism, Nat. Biotechnol. 31 (2013) 419–425, https://doi.org/10.1038/nbt.2488.
[44] N. Vlassis, M.P. Pacheco, T. Sauter, Fast reconstruction of compact context-specific metabolic network models, PLoS Comput. Biol. 10 (2014) e1003424, , https://doi.org/10.1371/journal.pcbi.1003424.
[45] H. Zur, E. Ruppin, T. Shlomi, iMAT: an integrative metabolic analysis tool, Bioinformatics 26 (2010) 3140–3142, https://doi.org/10.1093/bioinformatics/btq602.
[46] E. Bauer, J. Zimmermann, F. Baldini, I. Thiele, C. Kaleta, BacArena: individual-based metabolic modeling of heterogeneous microbes in complex communities, PLoS Comput. Biol. 13 (2017) e1005544, , https://doi.org/10.1371/journal.pcbi.1005544.
[47] D. Bates, M. Mächler, B. Bolker, S. Walker, Fitting linear mixed-effects models using lme4, J. Stat. Softw. 67 (2015) 1–48, https://doi.org/10.18637/jss.v067.i01.
[48] E. Faessler, U. Hahn, Semedico: a Comprehensive Semantic Search Engine for the Life Sciences, (2017).
[49] T. Kamisawa, T. Isawa, M. Koike, K. Tsuruta, A. Okamoto, Hematogenous metastases of pancreatic ductal carcinoma, Pancreas 11 (1995) 345–349.
[50] M.A. Kowalik, G. Guzzo, A. Morandi, A. Perra, S. Menegon, I. Masgras, E. Trevisan, M.M. Angioni, F. Fornari, L. Quagliata, G.M. Ledda-Columbano, L. Gramantieri, L. Terracciano, S. Giordano, P. Chiarugi, A. Rasola, A. Columbano, Metabolic reprogramming identifies the most aggressive lesions at early phases of hepatic carcinogenesis, Oncotarget 7 (2016) 32375–32393, https://doi.org/10.18632/oncotarget.8632.
[51] H. Zhao, L. Yang, J. Baddour, A. Achreja, V. Bernard, T. Moss, J.C. Marini, T. Tudawe, E.G. Seviour, F.A. San Lucas, H. Alvarez, S. Gupta, S.N. Maiti, L. Cooper, D. Peehl, P.T. Ram, A. Maitra, D. Nagrath, Tumor microenvironment derived exosomes pleiotropically modulate cancer cell metabolism, Elife 5 (2016), https://doi.org/10.7554/eLife.10250.
[52] T. Zhao, X. Mu, Q. You, Succinate: an initiator in tumorigenesis and progression, Oncotarget 8 (2017) 53819–53828, https://doi.org/10.18632/oncotarget.17734.
[53] P.-J. Aspuria, S. Lunt, L. Varemo, L. Vergnes, M. Gozo, J. Beach, B. Salumbides, K. Reue, W. Wiedemeyer, J. Nielsen, B. Karlan, S. Orsulic, Succinate dehydrogenase inhibition leads to epithelial-mesenchymal transition and reprogrammed carbon metabolism, Cancer Metabol. 2 (2014) 21, https://doi.org/10.1186/2049-3002-2-21.
[54] P.L. Tseng, W.H. Wu, T.H. Hu, C.W. Chen, H.C. Cheng, C.F. Li, W.H. Tsai, H.J. Tsai, M.C. Hsieh, J.H. Chuang, W.T. Chang, Decreased succinate dehydrogenase B in human hepatocellular carcinoma accelerates tumor malignancy by inducing the Warburg effect, Sci. Rep. 8 (2018) 3081, https://doi.org/10.1038/s41598-018-21361-6.
[55] D. Zhang, W. Wang, B. Xiang, N. Li, S. Huang, W. Zhou, Y. Sun, X. Wang, J. Ma, G. Li, X. Li, S. Shen, Reduced succinate dehydrogenase B expression is associated with growth and de-differentiation of colorectal cancer cells, Tumour Biol. 34 (2013) 2337–2347, https://doi.org/10.1007/s13277-013-0781-4.
[56] A. Viale, P. Pettazzoni, C.A. Lyssiotis, H. Ying, N. Sanchez, M. Marchesini, A. Carugo, T. Green, S. Seth, V. Giuliani, M. Kost-Alimova, F. Muller, S. Colla, L. Nezi, G. Genovese, A.K. Deem, A. Kapoor, W. Yao, E. Brunetto, Y. Kang, M. Yuan, J.M. Asara, Y.A. Wang, T.P. Heffernan, A.C. Kimmelman, H. Wang, J.B. Fleming, L.C. Cantley, R.A. DePinho, G.F. Draetta, Oncogene ablation-resistant pancreatic cancer cells depend on mitochondrial function, Nature 514 (2014) 628–632, https://doi.org/10.1038/nature13611.
[57] P. Sancho, E. Burgos-Ramos, A. Tavera, T. Bou Kheir, P. Jagust, M. Schoenhals, D. Barneda, K. Sellers, R. Campos-Olivas, O. Grana, C.R. Viera, M. Yuneva, B. Sainz Jr., C. Heeschen, MYC/PGC-1alpha balance determines the metabolic phenotype and plasticity of pancreatic cancer stem cells, Cell Metabol. 22 (2015) 590–605, https://doi.org/10.1016/j.cmet.2015.08.015.
[58] A. Rezza, R. Sennett, M. Rendl, Adult stem cell niches: cellular and molecular components, Curr. Top. Dev. Biol. 107 (2014) 333–372, https://doi.org/10.1016/B978-0-12-416022-4.00012-3.
[59] A. Marin-Hernandez, S. Rodriguez-Enriquez, P.A. Vital-Gonzalez, F.L. Flores-Rodriguez, M. Macias-Silva, M. Sosa-Garrocho, R. Moreno-Sanchez, Determining and understanding the control of glycolysis in fast-growth tumor cells. Flux control by an over-expressed but strongly product-inhibited hexokinase, FEBS J. 273 (2006) 1975–1988, https://doi.org/10.1111/j.1742-4658.2006.05214.x.
[60] Y. Song, Q. Luo, H. Long, Z. Hu, T. Que, X. Zhang, Z. Li, G. Wang, L. Yi, Z. Liu, W. Fang, S. Qi, Alpha-enolase as a potential cancer prognostic marker promotes cell growth, migration, and invasion in glioma, Mol. Canc. 13 (2014) 65, https://doi.org/10.1186/1476-4598-13-65.
[61] S.S. Ahmad, K. Glatzle, J. Fau - Bajaeifer, S. Bajaeifer, K. Fau - Buhler, T. Buhler S Fau - Lehmann, I. Lehmann T Fau - Konigsrainer, J.-P. Konigsrainer I Fau - Vollmer, B. Vollmer Jp Fau - Sipos, S.S. Sipos B Fau - Ahmad, H. Ahmad Ss Fau - Northoff, A.Northoff H. Fau - Konigsrainer, D. Konigsrainer A Fau - Zieker, D. Zieker, Phosphoglycerate kinase 1 as a promoter of metastasis in colon cancer, Int. J. Oncol. 43 (2013) 586–590, https://doi.org/10.3892/ijo.2013.1971.
[62] K. Liu, Z. Tang, A. Huang, P. Chen, P. Liu, J. Yang, W. Lu, J. Liao, Y. Sun, S. Wen, Y. Hu, P. Huang, Glyceraldehyde-3-phosphate Dehydrogenase Promotes Cancer Growth and Metastasis through Upregulation of SNAIL Expression vol. 50, (2017), pp. 252–262, https://doi.org/10.3892/ijo.2016.3774.